RESEARCH

Construction of a prognostic model for disulfidptosis-related long noncoding RNAs in R0 resected hepatocellular carcinoma and analysis of their impact on malignant behavior

Xuefeng Gu[1], Yanyan Wei[2], Duo Shen[3*] and Yuan Mao[4*]

Abstract

Background Disulfidptosis is an emerging form of cellular death resulting from the binding of intracellular disulfide bonds to actin cytoskeleton proteins. This study aimed to investigate the expression and prognostic significance of hub disulfidptosis-related lncRNAs (DRLRs) in R0 resected hepatocellular carcinoma (HCC) as well as their impact on the malignant behaviour of HCC cells.

Methods A robust signature for R0 resected HCC was constructed using least absolute shrinkage and selection operator (LASSO) and multivariate Cox regression and was validated in an independent internal validation cohort to predict the prognosis of R0 HCC patients. Comprehensive bioinformatics analysis was performed on the hub DRLRs (KDM4A-AS1, MKLN1-AS, and TMCC1-AS1), followed by experimental validation using quantitative real-time polymerase chain reaction (qRT–PCR) and cellular functional assays.

Results The signature served as an independent prognostic factor applicable to R0 HCC patients across different age groups, tumour stages, and pathological characteristics. Gene Ontology (GO) and gene set enrichment analysis (GSEA) revealed hub pathways associated with this signature. The high-risk group presented an increased abundance of M0 macrophages and activated memory CD4 T cells as well as elevated macrophage and major histocompatibility complex (MHC) class I expression. High-risk R0 HCC patients also presented increased tumour immune dysfunction and exclusion scores (TIDEs), mutation frequencies, and tumour mutational burdens (TMBs). Drug sensitivity analysis revealed that high-risk patients were more responsive to drugs, including GDC0810 and osimertinib. High expression levels of the three hub DRLRs were detected in R0 HCC tissues and HCC cell lines. Functional assays revealed that the three hub DRLRs enhanced HCC cell proliferation, migration, and invasion.

Conclusions A signature was constructed on the basis of three DRLRs, providing novel insights for personalized precision therapy in R0 HCC patients.

*Correspondence:
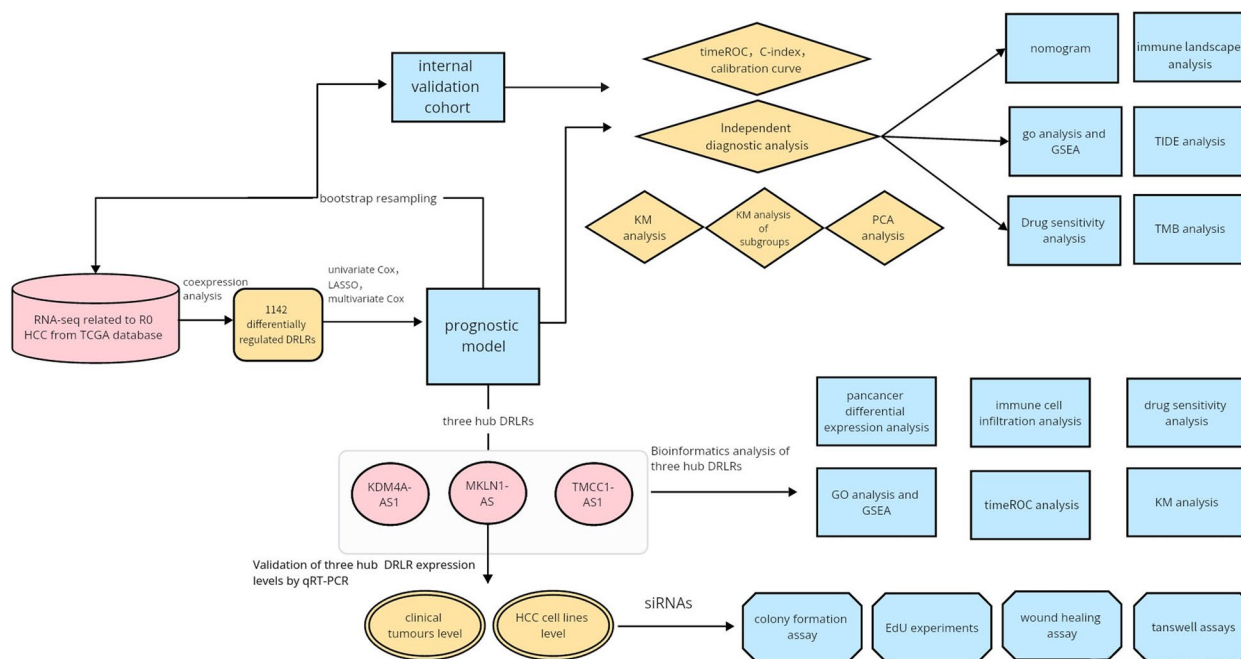Duo Shen
shenduo1991@163.com
Yuan Mao
ymaoent@njmu.edu.cn
Full list of author information is available at the end of the article

Gu *et al. BMC Cancer*   (2024) 24:1068

Page 2 of 19

Graphical Abstract

Background

Hepatocellular carcinoma (HCC) is one of the most prevalent malignancies globally, ranking sixth among all cancers. In 2020, an estimated 900,000 new cases and 830,000 deaths were reported, accounting for 4.7% and 8.3% of all malignant cancers, respectively [1]. HCC accounts for approximately 75%-85% of primary liver cancers [1]. Risk factors for HCC include chronic hepatitis (caused by hepatitis B or C virus infection), alcohol abuse, and metabolic syndrome [2]. Currently, diverse treatment modalities have been employed for HCC, including surgical resection, liver transplantation, ablation, transarterial chemoembolization, transarterial radioembolization, and systemic therapy [3, 4]. Nonetheless, owing to organ scarcity, stringent liver transplantation criteria, and a limited ablation range, liver resection remains the most frequently utilized curative method for early or partially intermediate HCC. However, the high rate of postoperative recurrence continues to impact the long-term overall survival (OS) of HCC patients, and the HCC recurrence rate within 5 years following liver resection is nearly 70% [5]. R0 resection denotes the absence of cancer cells along the resection margin in pathological sections. Currently, R0 resection remains the preferred treatment for early-stage HCC patients, as it is considered the primary curative approach associated with favourable long-term outcomes and the absence of recurrence [6]. Hence, achieving R0 resection should be pursued to achieve a satisfactory comprehensive treatment effect. Additionally, proactive treatment strategies, such as conversion therapy, aim to transform R1 and R2 resections into R0 resections, converting unresectable tumours into surgically curable ones and thus fulfilling the surgical criteria for safe R0 resection [7]. However, the 5-year survival rate following R0 resection remains limited to 40% to 65%. Recurrence affects more than half of the patients who undergo R0 resection [8], significantly compromising the long-term effectiveness of surgical intervention. Therefore, the exploration of potential therapeutic targets for R0 HCC holds tremendous clinical significance.

Disulfidptosis represents a novel mode of cell death distinct from traditional mechanisms [9]. Recent studies have revealed that during glucose deprivation, the abnormal accumulation of disulfides, such as cysteine, occurs within cells, triggering disulfide stress and

Gu *et al. BMC Cancer*   (2024) 24:1068

Page 3 of 19

increasing the content of disulfide bonds in the actin cytoskeleton, ultimately leading to cell death. The processes of intracellular disulfide bond formation and cleavage are closely associated with the onset and progression of cancer [10]. The disruption of disulfide metabolism also plays a role in promoting tumour cell proliferation, metastasis, and immune evasion in various biological processes [11, 12].

Currently, there is limited research on disulfidptosis-related lncRNAs (DRLRs) in tumours. Yang et al. [13] developed a prognostic model comprising 11 DRLRs and confirmed the significant promotion of invasive and migratory abilities in cancer cells by the DRLR OGFRP1. Liu et al. [14] established a novel DRLR model to predict the survival rate and chemotherapy drug sensitivity of cervical cancer patients, offering insights for personalized treatment approaches. However, few studies have investigated the prognostic relationship of DRLRs in HCC and their biological implications for tumour invasion and metastasis. Particularly for patients who have undergone more favourable R0 curative resection for HCC, the identification of new DRLR predictive models and biomarkers holds substantial clinical significance.

Artificial intelligence (AI) and machine learning (ML) are at the forefront of a healthcare revolution, facilitating sophisticated modelling of complex biological data and enhancing both diagnostic accuracy and treatment strategies. AI involves computer algorithms that mimic human cognitive functions, which are thriving on significant advancements in computational power and data availability. In medicine, AI applications include intelligent screening, diagnostics, risk prediction, and supportive care. Since the 1980s, the development of various ML algorithms, including decision trees, random forests, and support vector machines, has matured the field of medical AI. ML algorithms are categorized into supervised learning, unsupervised learning, and reinforcement learning, with ML being the most widely used AI technique today and developed using vast training datasets. Currently, the medical field leverages AI to automate various steps in clinical practice, supporting clinical decision-making. Implementing AI in medical domains not only heightens diagnostic precision but also reduces time and resource expenditures. The extensive application of AI technologies in medicine [15, 16] plays a pivotal role in early disease detection and intervention. In our research, AI and ML methodologies closely aligned with the analysis of DRLRs in HCC. AI and ML are used to categorize and assess large genomic datasets from The Cancer Genome Atlas (TCGA), enhancing analytical precision and advancing our understanding of HCC pathogenesis, potentially guiding personalized patient management and therapeutic strategies.

Given the pivotal role of R0 resection in HCC, coupled with the high recurrence rates observed in HCC patients post-R0 resection, this study aimed to identify prognostic lncRNA biomarkers associated with R0 HCC. The objective of this study was to identify additional therapeutic targets for R0 HCC treatment, ultimately aiding in the selection of appropriate pharmacological interventions for future applications. This investigation further introduces a newly discovered mode of programmed cell death termed disulfidptosis. Within the cohort of HCC patients who underwent curative R0 resection, we endeavoured to ascertain hub DRLRs through the robust construction of a prognostic risk model. This study focuses on examining potential biological pathways, immune landscapes, and clinical prognostic implications and influences the biological behaviour of HCC in association with these hub DRLRs. This foundation facilitates further exploration of the molecular mechanisms underlying hub DRLRs and their potential as therapeutic targets.

In this study, we conclusively identified the DRLRs that correlate with the prognosis of patients with R0 HCC. A prognostic risk model for DRLRs in R0 HCC patients was constructed via univariate Cox regression, least absolute shrinkage and selection operator (LASSO) regression, and multivariate Cox regression. We subsequently explored the biological enrichment analysis, immune microenvironment status, mutation profile, and drug treatment response in the patient risk groups within the model. Furthermore, we conducted a comprehensive examination of the clinical characteristics, immune cell infiltration features, drug sensitivity, and potential biological roles of the hub lncRNAs in the model. In summary, our study provides a robust prognostic model that offers valuable insights into the various prognoses and immune landscapes of R0 HCC patients, as well as potential therapeutic strategies. Additionally, we experimentally validated the oncogenic role of hub lncRNAs in promoting HCC cell proliferation, migration, and invasion in R0 HCC.

Methods

Data acquisition

We obtained transcriptomic data from 320 HCC tumour tissues and 50 adjacent normal liver tissues from patients who underwent curative resection with negative surgical margins (R0 resection) from TCGA database (https://portal.gdc.cancer.gov/). Tissue samples with a short-term survival of 0 years and incomplete survival data were excluded from the analysis. Further comprehensive clinical data were obtained from the cBioPortal database (http://www.cbioportal.org/). Using the Perl programming language (version Strawberry-5.30.1; https://www.perl.org), we processed the RNA sequencing (RNA-seq)

Gu *et al. BMC Cancer*   (2024) 24:1068

Page 4 of 19

data of R0 HCC samples, resulting in the identification of 16,876 lncRNAs and 19,938 mRNAs. Ten genes (GYS1, NDUFS1, OXSM, LRPPRC, NDUFA11, NUBPL, NCKAP1, RPN1, SLC3A2, and SLC7A11) were associated with disulfidptosis. To examine the correlation between these ten disulfidptosis-related genes and DRLRs, we performed rank-sum analysis via the Wilcoxon test. The expression levels of these ten genes were assessed for their associations with lncRNA expression levels using the wilcox.test() function in R. DRLRs with a correlation ($|cor|$) greater than 0.4 and a p value less than 0.001 were selected. Coexpression Sankey diagrams were constructed using the R packages "ggplot2" and "ggalluvial" to illustrate the coexpression patterns of the identified DRLRs and genes associated with disulfidptosis. As the patient information used in this study was obtained from TCGA database, we strictly followed the publication guidelines of TCGA; therefore, this study was exempt from ethical approval. Additionally, 18 HCC samples and corresponding adjacent normal tissues were collected from Jiangsu Provincial Cancer Hospital. Ethics approval was obtained from the ethics committee of Jurong Hospital affiliated to Jiangsu University (JRSRMYY-2023–042).

Construction and validation of prognostic lncRNAs for disulfidptosis

Initially, univariate Cox regression analysis was conducted to identify DRLRs significantly associated with OS in R0 HCC patients ($P < 0.05$). DRLRs with a significance level of $P < 0.05$ were further subjected to LASSO regression for dimensionality reduction. Multivariate Cox regression analysis based on the Akaike information criterion value was subsequently performed to select the most clinically valuable lncRNAs and establish a prognostic model. The risk score (RS) was calculated via the following formula: RS = (expression level of DRLR A × regression coefficient) + (expression level of DRLR B × regression coefficient) + …. To validate the obtained prognostic risk model, the bootstrap resampling method was utilized to establish an internal validation cohort consisting of 320 new R0 HCC patients. The bootstrap resampling method is widely recommended for the internal validation of prognostic models [17–19]. After the internal validation cohort was established, a chi-square test was employed to assess whether there were any differences in clinical characteristics between the training cohort and the internal validation cohort.

Using the median RS value as a threshold, the R0 HCC patients in the training cohort were subsequently stratified into high- and low-risk groups. Kaplan–Meier (KM) curve analysis was performed via the R packages "Survival" and "Survminer" to assess the survival disparities between the high- and low-risk groups. The R package "pheatmap" was employed to generate a risk score distribution of DRLRs within the model as well as a heatmap illustrating the expression risks of DRLRs corresponding to the survival status of each patient.

Furthermore, the applicability of the model across clinical characteristics was validated by employing KM curves to observe the disparities in OS between the high- and low-risk groups of R0 HCC patients with varying clinical features and pathological stages. Finally, the R package "timeROC" was utilized to generate a time-dependent receiver operating characteristic curve (timeROC) to assess the predictive performance of the prognostic model. Additionally, multi-ROC analysis was conducted to compare the predictive ability of the risk model with that of individual clinical variables and to observe the prognostic disparities between the risk model and single clinical variables. The R packages "dplyr", "rms", and "pec" were utilized to analyse the C-index, which assesses the probability of the model's predicted outcomes aligning with the actual observed outcomes. Principal component analysis (PCA) was performed to visualize the groups and determine whether the lncRNAs involved in constructing the model could effectively distinguish between the high- and low-risk groups.

Evaluation of the prognostic independence of a disulfidptosis risk model

Univariate and multivariate Cox regression analyses were performed to evaluate the independent prognostic factors, accounting for patient sex, age, histological grade, clinical tumour node metastasis (TNM) stage, and RS. The R package "rms" was employed to generate a nomogram for predicting the 1-year, 3-year, and 5-year survival rates of R0 HCC patients. Furthermore, a calibration curve was plotted to assess the concordance between the predicted values and the actual observed values.

Gene Ontology (GO) pathway enrichment analysis and gene set enrichment analysis (GSEA)

Gene expression in the high- and low-risk groups was compared to identify DEGs via the R package "limma" with the following criteria: log2 |fold change| > 1 and false discovery rate (FDR) < 0.05. GO analysis was conducted on the differentially expressed genes identified, and these genes are classified based on three components: biological process (BP), cellular component (CC), and molecular function (MF). The significant enrichment criteria for GO analysis were defined as $P < 0.05$ and FDR < 0.05. GSEA was performed on the high- and low-risk groups to explore the significantly enriched biological functions and pathways associated with R0 HCC. The gene sets selected for GSEA were c2.all.v2022.1.Hs.symbols.

Gu et al. BMC Cancer (2024) 24:1068

Page 5 of 19

gmt, c5.all.v2022.1.Hs.symbols.gmt, and h.all.v2022.1.Hs.symbols.gmt. A significance level of $P < 0.05$ and an FDR < 0.05 was considered statistically significant. The aforementioned enrichment analyses were conducted via the R packages "clusterProfiler", "org.Hs.eg.db", and "enrichment plot".

Tumour immune microenvironment, immunotherapy, and tumour mutation burden (TMB) analysis

To investigate the associations between risk scores and immune cells and their functions, we employed the R packages "limma," "reshape2," "ggpubr," "GSVA," "GSEA-Base," and "CIBERSORT." Single-sample gene set enrichment analysis (ssGSEA) and the CIBERSORT algorithm were utilized to evaluate the infiltration and functionality of tumour immune cells, and box plots were generated. The tumour immune dysfunction and exclusion (TIDE) algorithm was applied to simulate tumour immune escape mechanisms and predict the efficacy of immune therapy. Patient scores were calculated, and the response to immune therapy was analysed in two subgroups. Furthermore, the TMB and genetic variations across groups were assessed via the R package "maftools." We compared the differences in TMB between the high- and low-risk groups and generated waterfall plots for the top 15 genes with the highest mutation frequency in both groups. Finally, we performed an analysis of TMB and assessed the disparities in OS among R0 HCC patients on the basis of the combination of TMB and high-risk or low-risk groups.

Sensitivity analysis of potential drugs

The oncoPredict package [20] was employed to predict the therapeutic response of patients in the high-risk and low-risk groups to commonly used anticancer medications. The R packages "limma" and "ggpubr" were utilized to predict drug sensitivity by considering the half maximal inhibitory concentration (IC_{50}) and to assess the disparities in drug sensitivity between the high- and low-risk groups.

Hub DRLR bioinformatics analysis of the model

To validate the prognostic value of the DRLR model in R0 HCC, we conducted further bioinformatics analysis on the hub DRLRs within the constructed model. First, the R packages "limma," "plyr," "reshape2," and "ggpubr" were employed to perform pancancer analyses of the differential expression of hub DRLRs across 32 other cancer types. Subsequently, Pearson correlation analysis was performed using the R packages "limma," "tidyverse," "ggplot2," "ggpubr," "ggExtra," and "ComplexHeatmap" to identify significantly correlated coexpressed genes, which were visualized via a coexpression heatmap. The

selection criteria were a correlation coefficient > 0.4 and $p < 0.001$. The coexpressed genes were then subjected to GO enrichment analysis via R packages, and the hub DRLRs were categorized into high- and low-expression groups on the basis of the median expression for GSEA. The selection criteria were FDR < 0.05 and $P < 0.05$. R packages were utilized for drug sensitivity analysis and immune cell infiltration analysis for each hub DRLR. The R packages "ggplot2" and "reshape2" were employed to explore the expression levels of the three hub DRLRs in various clinical and pathological subgroups of R0 HCC patients in the risk model. Finally, on the basis of the median expression of prognostic hub DRLRs, the patients were divided into high- and low-expression groups, and KM survival analysis was conducted. Furthermore, the differences in expression between the hub DRLRs in R0 HCC patients and normal liver tissue were analysed, and receiver operating characteristic (ROC) and time-dependent ROC analyses were performed to assess their predictive performance.

Cell culture and quantitative real-time polymerase chain reaction (qRT–PCR) detection

In this study, we collected 18 pairs of clinical R0 HCC samples and their corresponding adjacent normal tissue samples. The expression of prognostic hub DRLRs was validated in HepG2, Hep3B2.1–7, and HCC-LM3 HCC cell lines, with the L02 cell line serving as the normal control for cell validation. The 18 pairs of R0 HCC samples and their corresponding adjacent normal tissue samples were obtained from Jiangsu Cancer Hospital. Total RNA was isolated and extracted via TRIzol reagent following the manufacturer's protocol, followed by cDNA synthesis. Finally, qRT–PCR experiments were performed using cDNA as a template. The relative expression levels of the hub DRLRs in the HCC cell lines and L02 cells were calculated using the $2 - \Delta\Delta Ct$ method, with glyceraldehyde-3-phosphate dehydrogenase (GAPDH) used as the reference gene. The primer sequences for the hub DRLRs and GAPDH are presented in Supplementary Table 1.

Cell proliferation assays

For the colony formation assay, 500 HCC cells were seeded into 6-well plates for culture. After 14 days, the HCC cells in the 6-well plates were fixed with 4% paraformaldehyde for 20 min and subsequently stained with 0.1% crystal violet solution for 15 min. For the 5-ethynyl-2'-deoxyuridine (EdU) experiment, HCC cells from different groups were cultured with 50 nmol/L EdU (RiboBio, China) for 2 h and fixed with 4% formaldehyde. Next, the cells were treated with 1 mL of Cell LightTM EdU Apollo 488 (RiboBio, China). Nuclear staining was achieved by treating the cells with DAPI for 30 min.

Gu *et al. BMC Cancer*   (2024) 24:1068

Page 6 of 19

Finally, the fluorescence intensity was measured via an inverted microscope.

Wound healing assay

HCC cells were cultured in 6-well plates. When the cell density was greater than 90%, a pipette tip was used to scratch the middle of each well. The cells were washed twice with phosphate buffer saline (PBS), and medium without foetal bovine serum (FBS) was added to each well. Images were obtained with an inverted microscope, and the distance between the two sides of the scratch was measured with a calliper. After 48 h of culture, the cells were photographed, and the distance was measured again.

Cell migration and invasion assays

Cell migration and invasion were assessed via Transwell chambers. For the cell invasion assay, 50 μL of Matrigel (BD Biosciences) was added to the upper chamber. After 24 h of incubation in the cell incubator, the migrated cells were fixed with 4% paraformaldehyde for 15 min and stained with 0.1% crystal violet for 15 min. Five images were randomly taken from each sample and counted.

Results

Construction and internal verification of a prognostic model based on DRLRs associated with poor prognosis in R0 HCC

After coexpression analysis, a total of 1142 differentially regulated DRLRs were identified (Fig. 1a). Subsequent univariate Cox regression analysis revealed 265 DRLRs with significant prognostic value. These DRLRs were then subjected to LASSO regression (Fig. 1b and c) and multivariate Cox regression analysis (Fig. 1d), resulting in the selection of 3 hub lncRNAs for inclusion in the prognostic model. The RS was calculated as follows: $RS = (0.48956 \times KDM4A\text{-}AS1$ expression$) + (0.28384 \times TMCC1\text{-}AS1$ expression$) + (0.36186 \times MKLN1\text{-}AS$ expression$)$. All 3 DRLRs included in the model were identified as risk factors. The correlation heatmap in Fig. 1e displays the associations between these DRLRs and disulfidptosis-related mRNAs. The training cohort and internal validation cohort
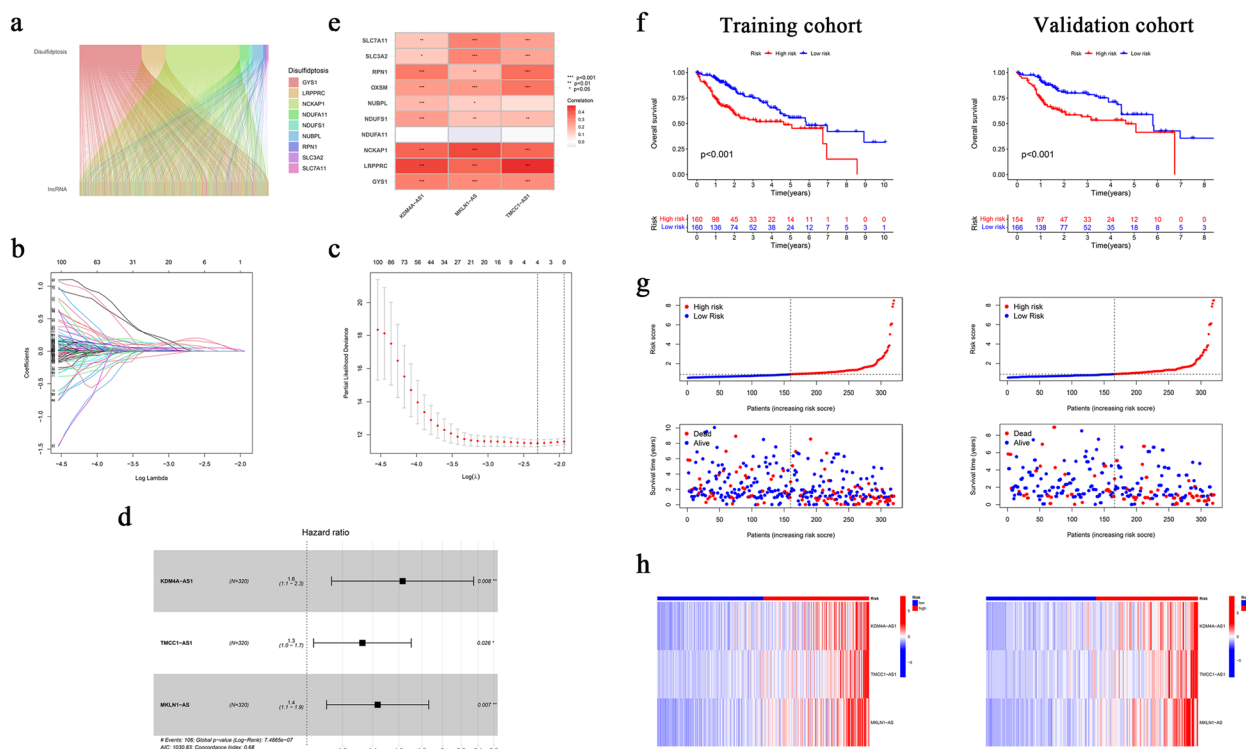

Fig. 1 Construction of an R0 hepatocellular carcinoma (HCC) prognostic necroptosis-related lncRNA (DRLR) risk model. **a** Sankey diagram of the coexpression of 9 disulfideptosis-related genes with 1142 DRLRs in R0 HCC. **b, c** Prognostic prediction model constructed via least absolute shrinkage and selection operator (LASSO)-Cox regression analysis. **d** Coexpression of 10 disulfideptosis-related genes and 3 prognostic hub disulfideptosis-related lncRNAs. **e** Coexpression of 10 disulfideptosis-related genes and 3 prognostic hub disulfideptosis-related lncRNAs. **f** Kaplan–Meier (KM) survival curves for the high-risk and low-risk groups in the training and validation cohorts. **g** Risk score distribution and survival status of HCC patients in the training and validation cohorts. **h** Risk heatmap of 3 hub prognostic DRLRs in the training and validation cohorts. Significant differences are indicated by *$P < 0.05$, **$P < 0.01$, and ***$P < 0.001$

Gu *et al. BMC Cancer* (2024) 24:1068

Page 7 of 19

presented comparable clinical characteristics (*P* > 0.05, Supplementary Table 2). R0 HCC patients in the high-risk group had significantly shorter OS than those in the low-risk group did. KM analysis of the internal validation cohort yielded consistent results (both *P* < 0.01) (Fig. 1f). Fig. 1g shows the distribution of RSs and the survival status of patients, indicating a higher mortality rate in the high-risk group among R0 HCC patients. The heatmap in Fig. 1h depicts the expression levels of the 3 hub DRLRs in the training and internal validation cohorts.

The disulfidptosis risk model predicts OS according to clinical characteristics

To evaluate the prognostic significance of the risk score for OS in R0 HCC patients with diverse clinical and pathological features, we stratified R0 HCC patients on the basis of age, sex, pathological grade, TNM stage, T stage, tumour family history, tumour vascular invasion,

and other variables. The outcomes (Fig. 2a-t) revealed that, within distinct subgroups, R0 patients classified in the high-risk group had significantly inferior OS compared with those classified in the low-risk group across the following subgroups: age < 60 years (*P* = 0.004), age ≥ 60 years (*P* = 0.010), male sex (*P* < 0.001), grade 1−2 (*P* = 0.001), stage I-II (*P* = 0.003), stage III-IV (*P* = 0.012), T1-2 stage (*P* = 0.005), T3-4 stage (*P* = 0.006), tumour family history (*P* = 0.035), no tumour family history (*P* = 0.003), tumour vascular invasion (*P* = 0.028), alpha-fetoprotein (AFP) levels ≥ 25 ng/mL (*P* = 0.002), serum albumin levels ≤ 4.0 g/dl (*P* < 0.001), Eastern Cooperative Oncology Group (ECOG) score < 1 (*P* = 0.022), and Eastern Cooperative Oncology Group (ECOG) score ≥ 1 (*P* = 0.021). These findings suggest that the DRLR risk model we developed effectively predicts the prognosis of R0 HCC patients within diverse clinical or pathological subgroups. Nevertheless, it is unfortunate that the
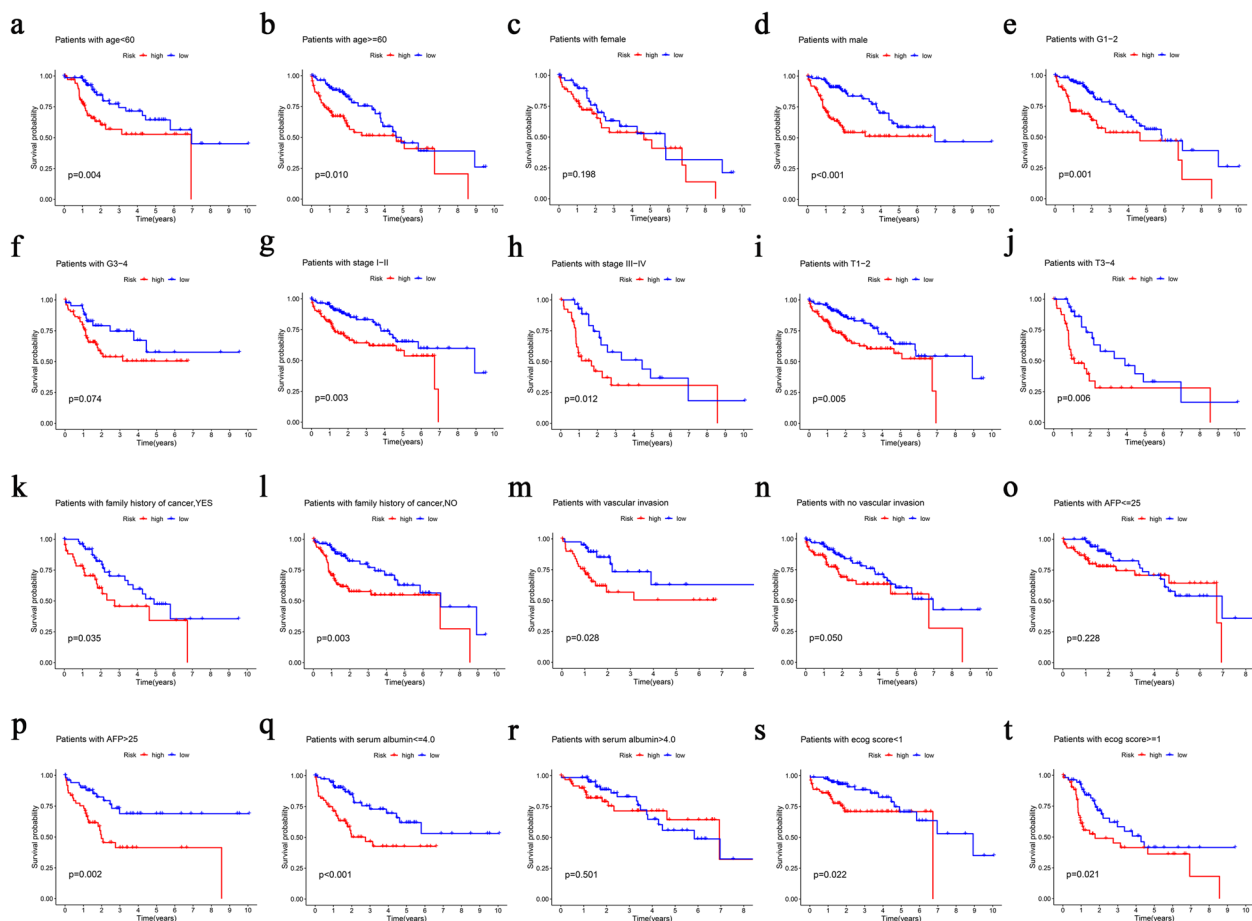

Fig. 2 KM survival curve analysis of overall survival (OS) between the high-risk and low-risk groups in the HCC clinicopathological feature subgroups via the 3-DRLR signature. **a** Age < 60 years, **b** Age ≥ 60 years, **c** Female, **d** Male, **e** Grade 1–2, **f** Grade 3–4, **g** Stage I-II, **h** Stage III-IV, (i) T1-2, **j** T3-4, **k** tumour family history, **l** no tumour family history, **m** vascular invasion, **n** no tumour vascular invasion, **o** alpha-fetoprotein (AFP) level ≤ 25 ng/mL, **p** AFP level > 25 ng/mL, **q** serum albumin level ≤ 4.0 g/dl, **r** serum albumin level > 4.0 g/dl, **s** Eastern Cooperative Oncology Group (ECOG) score < 1, **t** Eastern Cooperative Oncology Group (ECOG) score ≥ 1

prognostic value of the risk model was insufficient in the following subgroups: female, grade 3–4, no tumour vascular invasion, AFP levels < 25 ng/mL, and serum albumin levels > 4.0 g/dl. These results demonstrate the applicability of our 3-DRLR prognostic model for predicting the prognosis of R0 HCC patients with distinct clinical and pathological characteristics.

Identification of independent prognostic indicators

To validate whether the risk score and other clinical data can function as independent prognostic factors, we performed univariate and multivariate Cox regression analyses. The findings of the univariate analysis demonstrated that tumour TNM stage and the risk score were independent prognostic factors (Fig. 3a) ($P < 0.001$). The multivariate analysis findings revealed that the risk score remained an independent prognostic factor among the five clinical features (Fig. 3b) ($P < 0.001$). KM analysis of progression-free survival (PFS) in the

training cohort (Fig. 3c) and internal validation cohort (Fig. 3d) indicated that patients in the high-risk group with R0 HCC exhibited significantly shorter PFS than those in the low-risk group did ($P = 0.004$ and $P = 0.024$, respectively). The area under the curve (AUC) values for the prediction of the 1-, 2-, and 3-year survival rates of all patients using the prognostic model were 0.758, 0.685, and 0.624, respectively (Fig. 3e), suggesting that the prognostic model has greater predictive value for short-term overall survival at 1 year. The AUC for predicting the 1-year survival rate via the prognostic model was greater than that obtained for the independent prognostic factors of sex, age, histological grade, and tumour TNM stage, indicating that the constructed prognostic model outperformed these clinical parameters in survival prediction (Fig. 3f). Moreover, C-index analysis revealed that the RS exhibited significantly greater predictive ability than other clinical features did (Fig. 3g). A nomogram was created to predict the 1-,
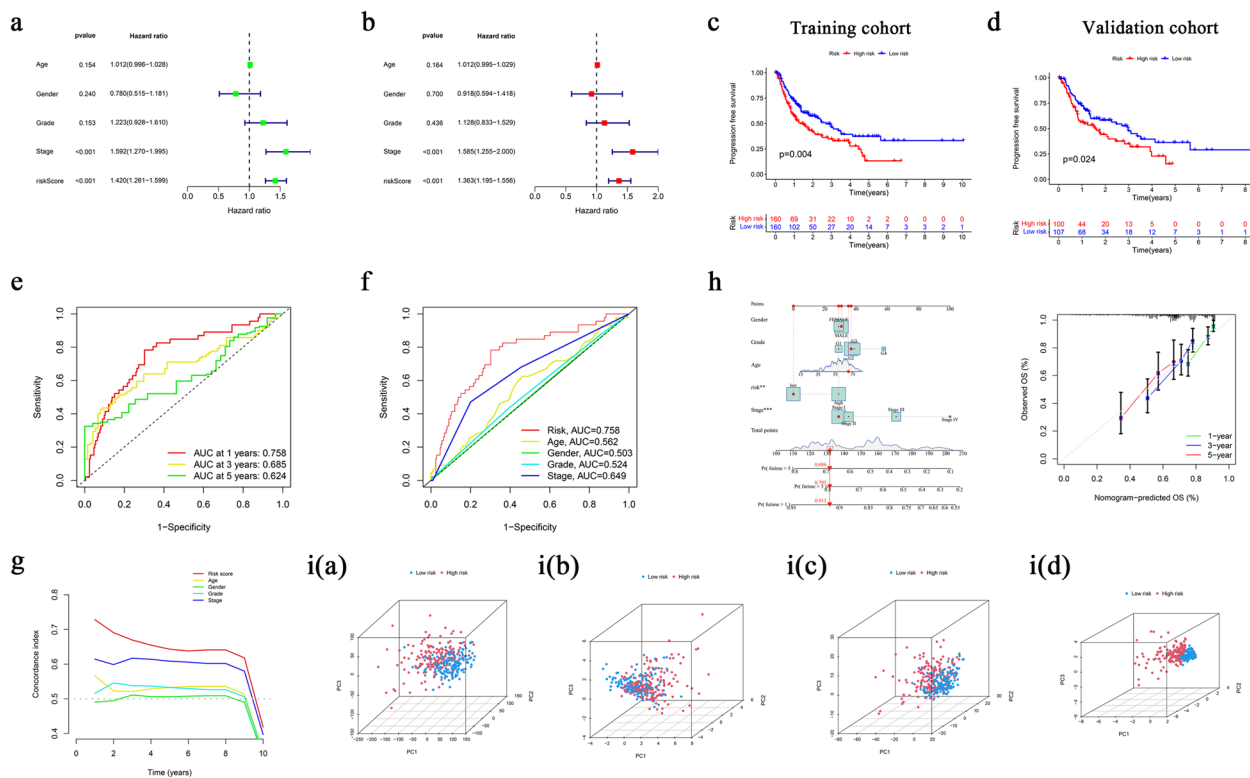
Fig. 3 Independent prognostic analysis, validation of the risk model and principal component analysis (PCA). **a** Univariate Cox analysis. Statistically significant differences in the TNM stage and risk score were noted. **b** Multivariate Cox analysis. Statistically significant differences in the TNM stage and risk score were noted. **c** KM survival curve of progression-free survival (PFS) for the high-risk and low-risk groups in the training cohort. **d** KM survival curve of PFS in the validation cohort. **e** A time-receiver operating characteristic (timeROC) curve was used to predict the 1-, 3-, and 5-year OS of R0 HCC patients. **f** MultiROC curve analysis revealed that the predictive accuracy of the risk model is superior to that of other clinical parameters. **g** C-index showing that the predictive accuracy of the risk model is superior to that of other clinical parameters. **h** Nomogram for predicting prognosis based on the 3-DRLR signature score and calibration curve for predicting 1-year, 3-year, and 5-year overall survival. PCA between the high-risk and low-risk groups was performed on the basis of (ia) all genes, (ib) disulfideptosis-related genes, (ic) DRLRs, and (id) 3-DRLR prognostic markers

3-, and 5-year survival rates of patients on the basis of the RS, age, sex, pathological characteristics, and TNM tumour stage (Fig. 3h). As an example of a clinical application, the corresponding score for the 20th patient was 132. According to this score, the patient's estimated survival rates at 1, 3, and 5 years were 91.3%, 79.5%, and 68.6%, respectively. The calibration curve demonstrated concordance between the predicted and actual survival rates (Fig. 3h). These findings substantiate the stability and accuracy of the nomogram, which integrates the clinical features and prognostic features of DRLRs, enabling the clinical application of this tool for monitoring R0 HCC patients. The PCA results revealed effective discrimination between the high- and low-risk groups using the prognostic model (Fig. 3i(d)), which surpassed the performance of the models based on all the genes (Fig. 3i(a)), disulfidptosis-related genes (Fig. 3i(b)), and DRLRs (Fig. 3i(c)).

GO analysis and GSEA of risk DEGs

A GO pathway analysis was conducted to perform a functional enrichment analysis of the 1,345 genes that were differentially expressed between the high- and low-risk groups. Significant enrichment was detected for BPs, including nuclear division, chromosome segregation, organelle fission, mitotic nuclear division, and nuclear chromosome segregation (Fig. 4a, b). GSEA was performed on the high-risk and low-risk groups of R0 HCC patients, which were classified on the basis of their prognostic risk scores. The results revealed that the gene sets in the high-risk group were significantly enriched in processes such as andersen cholangiocarcinoma class 2 and basaki ybx1 targets up within the c2.all.v2022.1.Hs.symbols.gmt gene set (Fig. 4c). Conversely, the genes in the low-risk group were primarily involved in pathways such as fatty acid metabolism and poor survival in the low-risk group as demonstrated by KEGG pathway analysis (Fig. 4d). For the c5.all.v2022.1.Hs.symbols.gmt gene set, the high-risk group was predominantly associated with pathways such as gobp regulation of animal organ morphogenesis and the external encapsulating structure (Fig. 4e). In contrast, the low-risk group was primarily involved in pathways such as gobp mitochondrial electron transport of cytochrome c to oxygen and high-density lipoprotein particles (Fig. 4f). For the h.all.v2022.1.Hs.symbols.gmt gene set, the gene sets in the high-risk group demonstrated significant enrichment in pathways such as hallmark e2f targets and hallmark epithelial mesenchymal transition (Fig. 4g). Conversely, the gene sets in the low-risk group presented no significant pathway enrichment.

Immune landscape analysis of the high- and low-risk groups in the model

Immune infiltration analysis revealed a significant increase in the abundance of M0 macrophages and memory CD4 T cells activated in the R0 HCC high-risk group compared with the low-risk group. Conversely, the abundances of resting memory CD4 T cells, activated natural killer (NK) cells, and monocytes were significantly lower in the high-risk group than in the low-risk group (Fig. 5a). The immune function score revealed that the number of macrophages and major histocompatibility complex (MHC) class I expression were significantly greater in R0 HCC patients in the high-risk group than in those in the low-risk group. On the other hand, B cells, cytolytic activity, mast cells, neutrophils, NK cells, plasmacytoid dendritic cells (pDCs), tumour infiltrating lymphocytes (TILs), the type I interferon (IFN) response, and the type II IFN response were significantly lower in the high-risk group than in the low-risk group of R0 HCC patients (Fig. 5b). Our findings provide valuable insights into the potential of immunotherapy for R0 HCC patients. Finally, the TIDE score significantly differed between the high-risk and low-risk groups, indicating that immunotherapeutic efficacy was superior in the low-risk group compared with the high-risk group ($P < 0.001$, Fig. 5g).

Analysis of the TMB of the 3-DRLR risk model in R0 HCC patients

The waterfall plot illustrates the top 15 genes with the highest mutation frequencies in both groups. Fig. 5c, d shows mutation rates of 86.08% and 76.13% in the high- and low-risk cohorts, respectively. TP53 presented the highest mutation score in the high-risk group, whereas TTN presented the highest mutation score in the low-risk group. Furthermore, compared with patients in the low-risk cohort, those in the high-risk cohort had significantly increased frequencies of mutations in TP53, CTNNB1, MUC16, PCLO, RYR2, APOB, LRP1B, XIRP2, CSMD3, ABCA13, OBSCN, and FLG. Conversely, the mutation frequencies of TTN and ALB showed the opposite trend. KM curve analysis indicated that R0 HCC patients with high TMB had significantly lower overall survival than those with low TMB (Fig. 5e, 5 = 0.003). Combined survival analysis using TMB and RSs yielded composite survival curves. The population was divided into four groups according to the median RS and median TMB: high TMB + high risk, high TMB + low risk, low TMB + high risk, and low TMB + low risk. Among these groups, patients with low TMB + low risk presented the most significant survival advantage, whereas those with high TMB + high risk presented the poorest overall survival rate (Fig. 5f).
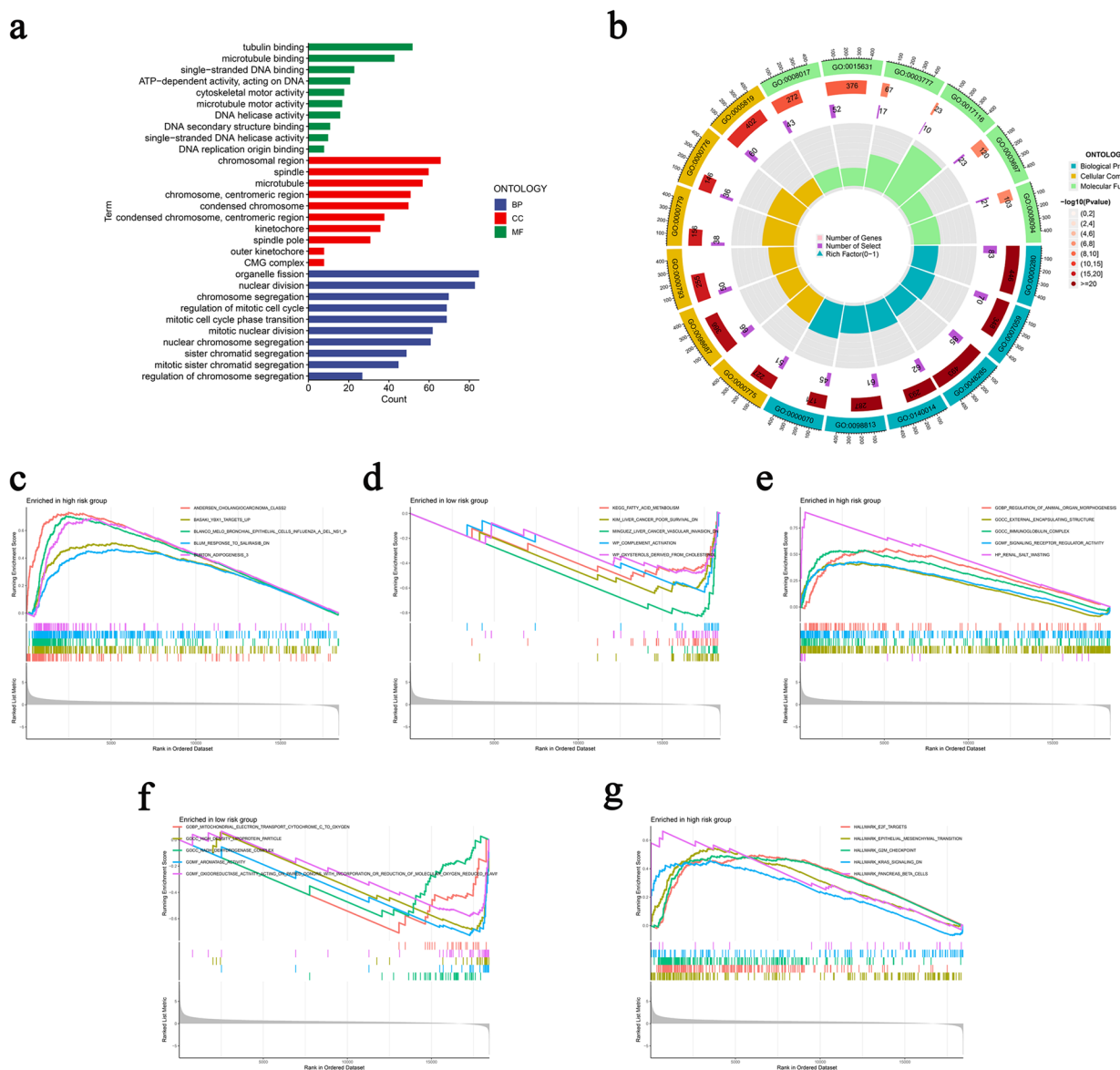
Fig. 4 Gene Ontology (GO) and gene set enrichment analysis (GSEA). **a** Bar chart of the top 10 enriched GO terms. **b** Circle diagram of the GO enrichment analysis results. GSEA revealed significant differences in enrichment in the TCGA R0 HCC cohort for the c2.all.v2022.1.Hs.symbols. gmt gene set between the 3-DRLR signature high-risk group (**c**) and low-risk group (**d**) and for the c5.all.v2022.1.Hs.symbols.gmt gene set between the high-risk group (**e**) and low-risk group (**f**). Significant enrichment in the h.all.v2022.1.Hs.symbols.cmt gene set was found in the high-risk group (**g**)

Drug sensitivity analysis of R0 HCCs

The oncoPredict package was utilized to predict the IC_{50} scores of R0 HCC patients in response to anticancer drug therapies. The findings revealed that patients in the high-risk group displayed heightened sensitivity to drugs such as GDC0810 (Fig. 6a), MK-8776 (Fig. 6b), osimertinib (Fig. 6c), paclitaxel (Fig. 6d), and YK-4–279 (Fig. 6e). Conversely, patients in the low-risk group demonstrated increased sensitivity to drugs,

including JAK1_8709 (Fig. 6f), JQ1 (Fig. 6g), Nutlin-3a (-) (Fig. 6h), PF-4708671 (Fig. 6i), and SB505124 (Fig. 6j).

## Bioinformatics analysis of the hub DRLRs in the risk model

The three hub DRLRs in our constructed risk model were further subjected to pancancer differential expression analysis of 32 cancer types from TCGA database. The results are shown in Supplementary Figs. 1a. Further
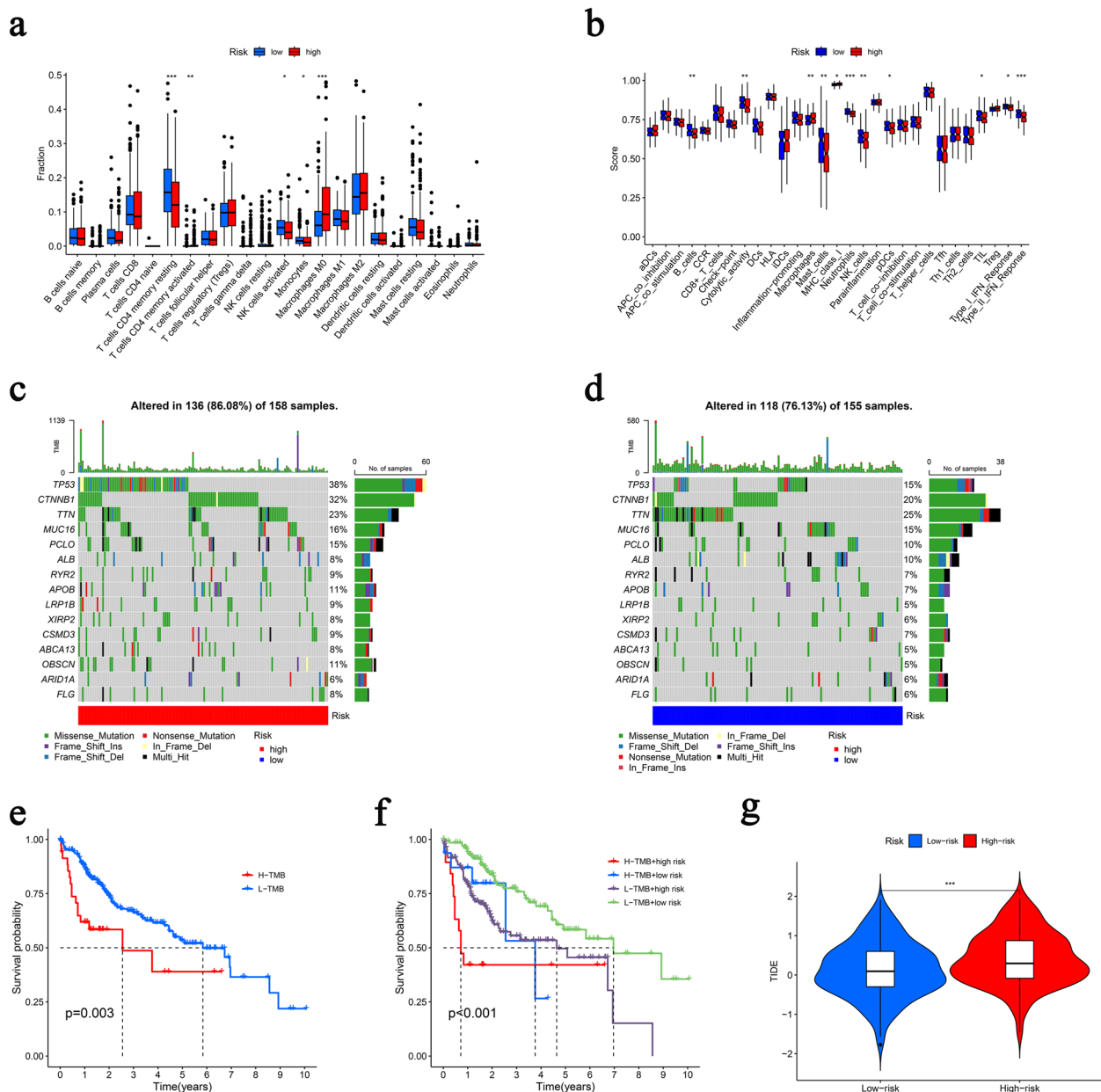
Fig. 5 Immune landscape of HCC patients and the relationship between tumour mutation burden (TMB) and the risk score. **a** Percentages of 22 immune cells in the high- and low-risk groups were calculated via the CIBERSORT algorithm. **b** Immune function scores of patients in the high- and low-risk groups. **c**, **d** Waterfall charts of somatic mutation features for both groups. **e** KM survival curves of the high- and low-TMB groups. **f** KM survival curves of the four groups. **g** Analysing immune escape on the basis of tumour immune dysfunction and exclusion (TIDE) scores. Significant differences are indicated by *$P < 0.05$, **$P < 0.01$, and ***$P < 0.001$

coexpression analysis identified genes that were coexpressed with the three hub lncRNAs used in the risk model, suggesting their potential regulatory value. The heatmap displays the top 50 most significant genes (Supplementary Fig. 1d-f). GO analysis revealed significantly enriched pathways and processes associated with the genes coexpressed with the three hub DRLRs

(Supplementary Figs. 2–4). GSEA confirmed the involvement of active functional pathways in the groups with high and low expression of the three hub DRLRs (Supplementary Figs. 2–4). Spearman correlation analysis revealed a relationship between the expression of the three hub DRLRs and immune cell infiltration (supplementary Fig. 1 g-f). Finally, we examined the drug sensitivity of the three

Gu *et al. BMC Cancer*   (2024) 24:1068

Page 12 of 19
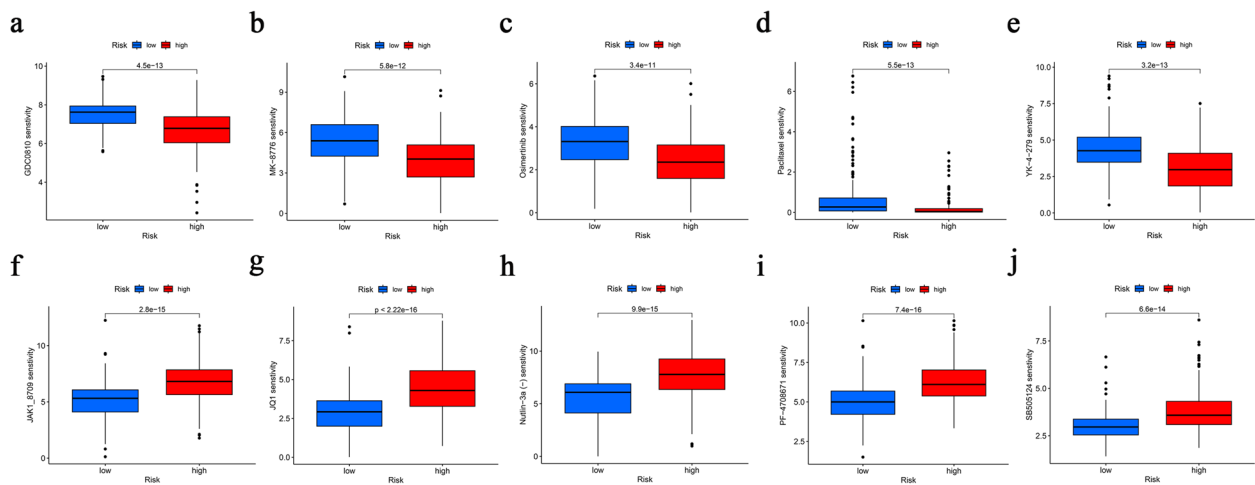
Fig. 6 Drug sensitivity of HCC patients in the high-risk and low-risk groups on the basis of the 3-DRLR signature. The top 5 drugs in terms of drug sensitivity and drug resistance are shown. The HCC patients in the high-risk group were more sensitive to (**a**) GDC0810, (**b**) MK-8776, (**c**) osimertinib, (**d**) paclitaxel, and (**e**) YK-4–279 and more resistant to (**f**) JAK1_8709, (**g**) JQ1, (**h**) Nutlin-3a (-), (**i**) PF-4708671, and (**j**) SB505124
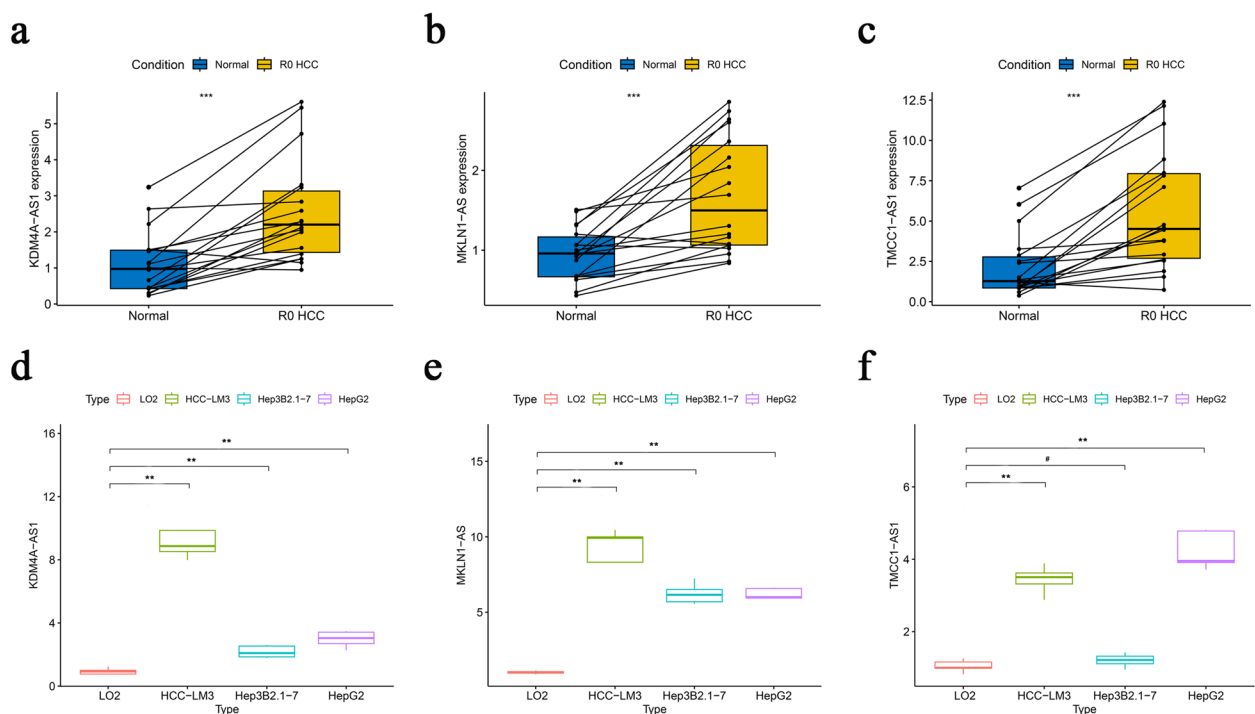
Fig. 7 Validation of prognostic hub lncRNA expression levels in the 3-DRLR model in clinical samples and HCC cell lines. KDM4A-AS1 (**a**), MKLN1-AS (**b**), and TMCC1-AS1 (**c**) expression levels in paired clinical samples of R0 HCC and paracancerous tissues. KDM4A-AS1 (**d**), MKLN1-AS (**e**), and TMCC1-AS1 (**f**) expression levels in the HCC cell lines HepG2, Hep3B2.1–7, and HCC-LM3 and normal liver tissue L02. Significant differences are indicated by *$P < 0.05$ and **$P < 0.01$, whereas # denotes no significant difference

hub DRLRs in the risk model, and the top 5 drugs in terms of sensitivity and resistance are shown in Supplementary Figs. 5–7, providing valuable insights for drug development. The expression levels of the three hub DRLRs in the risk model were found to be associated with the clinical and pathological characteristics of R0 HCC patients (Supplementary Fig. 8a-k). These three hub DRLRs were significantly differentially expressed in terms of pathological grade, TNM stage, and survival status. R0 HCC patients with high expression of the hub DRLRs exhibited

Gu *et al. BMC Cancer* (2024) 24:1068

Page 13 of 19
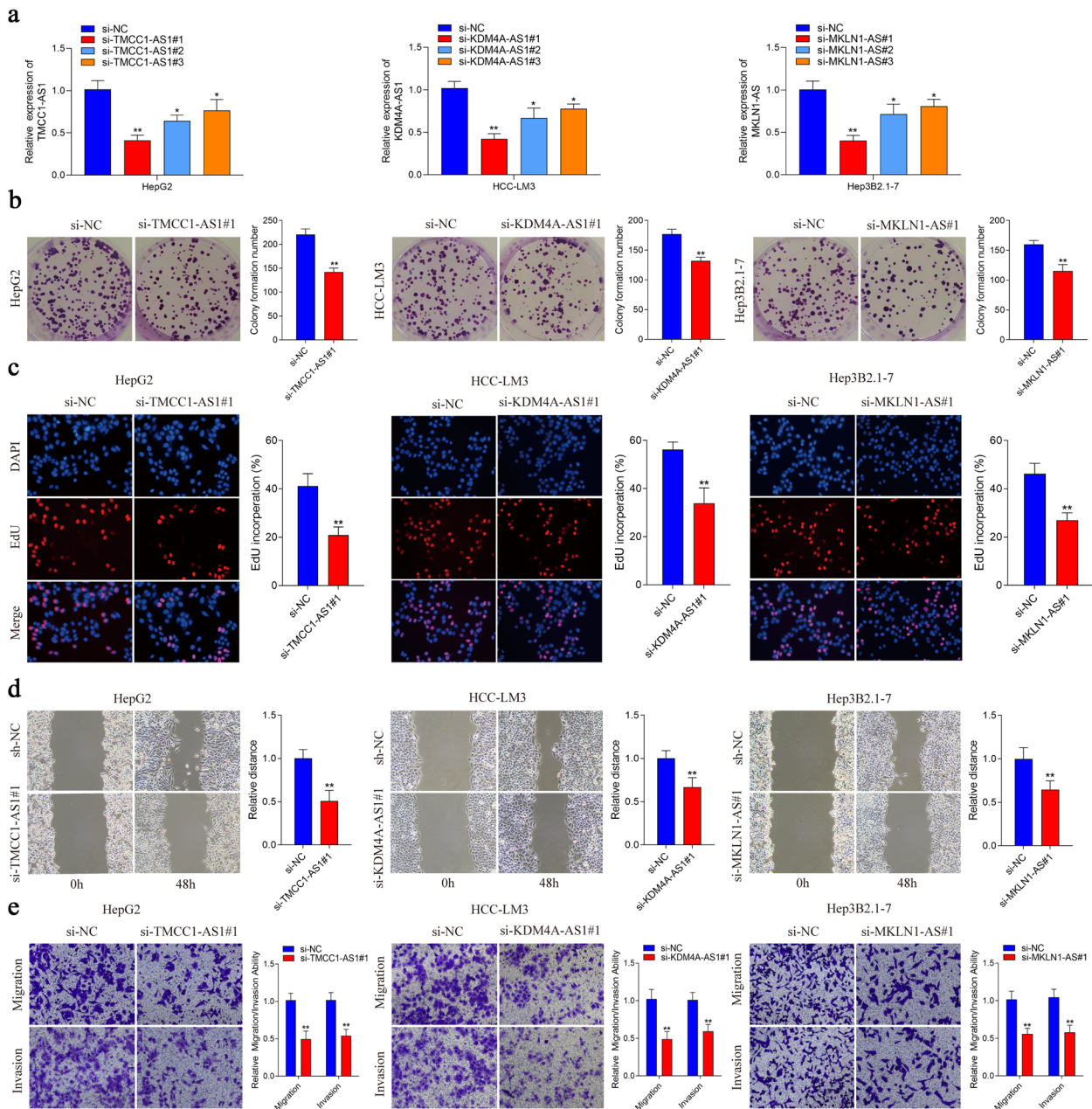
Fig. 8 Effects of three hub lncRNAs on the biological functions of HCC cells in vitro. The knockdown efficiency in HepG2, HCC-LM3 and Hep3B2.1-7 cells was detected using quantitative real-time polymerase chain reaction (qRT–PCR) (**a**). Colony formation assay of HCC cells transfected with si-NC and si-RNA (**b**). EdU assay of HCC cells transfected with si-NC and si-RNA (**c**). Wound healing assay of HCC cells transfected with si-NC and si-RNA (**d**). Transwell assays of HCC cells transfected with si-NC and si-RNA (**e**). Significant differences are indicated by *$P < 0.05$ and **$P < 0.01$.

significantly shorter survival (Supplementary Fig. 9a-c). The timeROC analysis comprehensively assessed the prognostic accuracy of the three hub DRLRs and revealed that they had greater predictive value for short-term overall survival at one year (Supplementary Fig. 9d-f). Additionally, the expression levels of the three hub DRLRs in R0 HCC patients were significantly greater than those in adjacent normal tissues (Supplementary Fig. 10a-c). Further ROC analysis was conducted to evaluate the ability of these three hub DRLRs to distinguish R0 HCC from normal tissues (Supplementary Fig. 10d-f). These results indicate that the expression levels of the three hub DRLRs exhibit good discriminatory power and high diagnostic value for R0 HCC.

Validation of hub DRLR expression levels in the risk model

The expression of the three hub DRLRs in paired samples of clinical tumours and adjacent tissues was analysed via qRT−PCR. The results demonstrated that KDM4A-AS1, MKLN1-AS, and TMCC1-AS1 expression levels were significantly greater in R0 HCC than in adjacent tissues (Fig. 7a-c). Furthermore, the expression of these three hub DRLRs was assessed in three HCC cell lines (HepG2, HCC-LM3, and Hep3B2.1–7) and a normal liver cell line (L02) via qRT−PCR. The findings revealed that both KDM4A-AS1 and MKLN1-AS expression was higher in all three HCC cell lines than in the normal liver cell line L02 (Fig. 7d-f). Moreover, the expression of these DRLRs was significantly greater in the highly invasive HCC-LM3 cell line than in the Hep3B2.1–7 and HepG2 cell lines, both of which exhibit considerably lower levels of invasiveness. Conversely, although TMCC1-AS1 expression was significantly elevated in HepG2 and HCC-LM3 cells compared with L02 cells, TMCC1-AS1 expression was not significantly altered in the Hep3B2.1–7 HCC cell line. Additionally, the increase in TMCC1-AS1 expression in the highly invasive HCC-LM3 cell line was less pronounced than that in the HepG2 cell line. These findings suggest that TMCC1-AS1 expression and function may be influenced by tissue specificity and HCC cell specificity. These results provide initial evidence that our risk-associated hub DRLRs not only are highly expressed in HCC but also may play a role in regulating the malignant biological behaviour of HCC cells. Therefore, we will employ in vitro experiments to silence the expression of the three hub DRLRs and investigate their impact on HCC cell proliferation, migration, and invasion.

The effects of hub DRLRs on the biological functions of HCC cells in vitro

TMCC1-AS1, KDM4A-AS1 and MKLN1-AS expression was knocked down via small interfering RNAs (siRNAs), and the relative lncRNA expression in HCC cells was measured via qRT−PCR (Fig. 8a). The siRNA with the most significant knockdown efficiency was selected for subsequent functional experiments. To test the proliferative capacity of the HCC cells, we performed a colony formation assay. The results revealed that the number of clones formed by the si-TMCC1-AS1, si-KDM4A-AS1 and si-MKLN1-AS groups was significantly lower than that formed by the control group (Fig. 8b). We also further verified the proliferative capacity of the HCC cells by performing EdU experiments (Fig. 8c). The results of these experiments revealed that the knockdown of TMCC1-AS1, KDM4A-AS1 and MKLN1-AS expression significantly inhibited the proliferative capacity of HCC cells. To assess the invasion and migration ability of HCC cells

after the knockdown of TMCC1-AS1, KDM4A-AS1 and MKLN1-AS, we performed wound healing and Transwell assays. In the wound healing assay, the si-TMCC1-AS1, si-KDM4A-AS1 and si-MKLN1-AS groups presented significantly decreased migration ability compared with the control group (Fig. 8d). Transwell assays revealed that invasion and migration were inhibited in the si-TMCC1-AS1, si-KDM4A-AS1 and si-MKLN1-AS groups (Fig. 8e).

Discussion

R0 resection is the most effective treatment for HCC, with significantly higher survival rates observed in patients who undergo surgical resection than in those who are ineligible for surgery. However, the rate of recurrence in patients who undergo curative liver resection remains high [21], with a higher risk of postoperative recurrence within the first year [22]. Therefore, identifying effective early diagnostic and prognostic factors is crucial. In recent years, our understanding of cell death mechanisms has improved. The discovery of new programmed cell death pathways has broadened our understanding of tumour occurrence and development and has provided new prospects for treatment. Disulfide-induced cell death, known as disulfidptosis, is distinct from well-known forms of cell death, such as ferroptosis, necrotic apoptosis, apoptosis, and pyroptosis. It represents a novel cell death pathway that lacks common features observed in other forms of cell death, such as caspase-3 cleavage or adenosine 5'-triphosphate (ATP) depletion, and is not associated with the formation of cysteine crystals in the context of cystinuria or cystinosis [23, 24]. Disulfidoptosis is characterized by the excessive accumulation of intracellular disulfide molecules and the depletion of nicotinamide adenine dinucleotide phosphate (NADPH), with disulfide stress inducing cell death [9]. Disulfides, as crucial regulators of oxidative metabolism, can influence various cellular activities in tumour cells, including survival and metastasis [25]. Aberrant regulation of disulfidptosis may also contribute to tumour progression and drug resistance [26]. Understanding the intricate mechanisms controlling these pathways provides new strategies for the development of innovative therapeutic approaches targeting disulfidptosis [27, 28].

In our study, we developed a prognostic risk model for R0 HCC patients incorporating three differentially expressed lncRNAs known as hub DRLRs (KDM4A-AS1, MKLN1-AS, and TMCC1-AS1). This model demonstrated the ability to predict the risk of mortality, OS, and PFS in R0 HCC patients, with improved outcomes observed in the low-risk group. Currently, few DRLR models have been constructed for HCC patients, particularly prognostic models involving lncRNAs, which could

Gu *et al. BMC Cancer* (2024) 24:1068

Page 15 of 19

offer a novel perspective for targeted tumour therapy focused on lncRNAs.

Prior investigations have indicated that KDM4A-AS1 promotes in vitro proliferation, migration, and invasion of liver cancer cells as well as in vivo liver cancer growth and lung metastasis through the KDM4A-AS1/KPNA2/HIF-1α pathway [29]. Shen et al. [30] demonstrated that KDM4A-AS1 facilitates tumour formation in vivo via the phosphoinositide 3-kinase (PI3K)/protein kinase B (AKT) pathway. Moreover, the peptide encoded by KDM4A-AS1 attenuates the viability and migratory capacity of oesophageal squamous cell carcinoma cells and plays a role in fatty acid metabolism and redox processes [31]. Our qRT−PCR experiments revealed elevated expression of KDM4A-AS1 in clinical samples and HCC cell lines. Additionally, in vitro functional assays confirmed the malignant biological behaviour of KDM4A-AS1 in promoting HCC cell proliferation, migration, and invasion. These findings are consistent with previous research conducted on HCC. Similarly, MKLN1-AS depletion leads to reduced viability, proliferation, and invasion and attenuated epithelial−mesenchymal transition (EMT) effects in HCC cells, suggesting that MKLN1-AS is transcriptionally regulated by SOX9 and mediates the influence of SOX9 on HCC cell proliferation and EMT [32]. Chen et al. [33] reported a correlation between the upregulation of MKLN1-AS and vascular invasion, decreased disease-free survival, and OS in HCC patients. Notably, MKLN1-AS knockout significantly inhibited HCC cell migration and growth and enhanced the proapoptotic effect of lenvatinib. Additionally, MKLN1-AS promotes in vivo HCC tumour growth through modulation of the miR-22-3p/E-twenty-six (ETS)1 axis [34] and the MKLN1-AS/miR-654-3p/hepatoma-derived growth factor (HDGF) axis [35]. These findings are consistent with our conclusions and lend support to our research results. Furthermore, TMCC1-AS1 has been linked to OS [36, 37] and recurrence-free survival in patients with HCC [38]. Fu et al. [39] discovered that TMCC1-AS1 is important in constructing a predictive model for the early recurrence of HCC, and a nomogram combining TMCC1-AS1 with AFP and TNM clinicopathological features can guide clinical decision-making. A study conducted by Chen et al. [40] also demonstrated that TMCC1-AS1 knockdown significantly inhibited the proliferation, migration, and invasion of HepG2 and SNU-182 cells, whereas TMCC1-AS1 over-expression had the opposite effect. TMCC1-AS1 promotes HCC cell proliferation, migration, and invasion through EMT. Our findings are consistent with those of previous studies, indicating that TMCC1-AS1 knockdown suppresses HCC cell proliferation, migration, and invasion.

On the basis of the RS, we further compared the immune microenvironments in the high-risk and low-risk groups using the model. The results revealed significantly enhanced immune functions, such as macrophages and MHC class I, in the high-risk group. Conversely, immune cell infiltration analysis revealed significant enrichment of M0 and T memory-activated immune cells in the high-risk group, whereas CD4 memory resting T cells, activated NK cells, and monocytes were more abundant in the low-risk group. This difference may be attributed to T-cell exhaustion caused by prolonged exposure to persistent antigens and inflammatory environments in R0 HCC patients, resulting in the loss of memory T-cell characteristics and the emergence of T-cell exhaustion, reducing the antitumour ability of the tumour [41]. Our study indicated that the high-risk group presented a higher TMB than did the low-risk group. The high-risk group also presented a significantly greater frequency of TP53 mutations, and TP53 presented the greatest difference in mutation frequency. Previous studies have also demonstrated a positive correlation between TP53 mutation and prognosis in patients with HCC [42]. Our survival analysis further revealed that the best prognosis was associated with low TMB combined with a low risk score. Future research should investigate whether the poor prognosis can be attributed to increased TP53 mutations. In the experimental validation section of this study, we confirmed the high expression of three hub DRLRs (KDM4A-AS1, MKLN1-AS, and TMCC1-AS1) in R0 HCC clinical specimens and HCC cell lines via qRT−PCR. Clonogenic, EdU, cell scratch, and Transwell assay results demonstrated that KDM4A-AS1, MKLN1-AS, and TMCC1-AS1 knockdown increased HCC cell proliferation and inhibited their migration and invasion. The downregulation of these three hub DRLRs affects the malignant biological behaviour of HCC cells, suggesting that they may serve as candidate targets for the prognosis and treatment of HCC patients.

Recently, the landscape of medical treatment for HCC has undergone significant transformations, particularly in the areas of immunotherapy and predictors of therapeutic response. Recent scientific literature illustrates a perceptible shift towards integrated treatment modalities that synergistically blend immune checkpoint inhibitors (ICIs) with traditional therapies. For instance, the emergence of locoregional and systemic therapy combinations — notably trans-arterial chemoembolization paired with ICIs — underscores a clinical paradigm favouring a collective assault on tumour sites, aiming to potentiate antitumoural responses [43]. Parallel to this evolving therapeutic landscape, the pressing need for reliable prognostic indicators to tailor treatment is well recognized. The utility of the ALB level as a prognostic

Gu *et al. BMC Cancer*   (2024) 24:1068

Page 16 of 19

biomarker is supported by robust data indicating a clear inverse relationship between the ALB level and survival outcome in patients receiving ICI treatment [44]. This finding not only reveals the potential of albumin levels for stratifying patient prognosis but also potentially guides dietary and management decisions to mitigate hypoalbuminaemia. Moreover, the Royal Marsden Hospital (RMH) score, which has been identified for its prognostic value, has emerged as a vital tool, deploying simple yet effective clinical markers to predict treatment outcomes across various cancers, including HCC [45]. This prognostic tool facilitates more nuanced clinical decisions, optimizing treatment trajectories in a complex therapeutic field marked by the advent of immune modulation strategies. Despite these advancements, challenges persist, notably in the form of treatment-induced adverse effects such as hepatic toxicity. Insightful data demonstrate heightened risks of hepatic enzyme elevation with ICI use, necessitating vigilant hepatic monitoring and possibly precluding specific patient demographics from such treatments owing to risk factors [46]. In HCC, advancing immune therapy involves recognizing its diverse response landscape. Recent data from the MOUSEION-02 study illuminate significant implications regarding neurotoxicity risks in immunotherapy [47]. Critically, understanding these markers not only promotes safer patient management but could also lead to the adjustment of therapeutic paradigms, potentially influencing survival outcomes in HCC patients receiving these treatments. These findings invite further examination of the predictive factors contributing to adverse responses, which are essential for optimizing HCC immunotherapy efficacy. Taken together, these insights suggest a dual strategy for HCC management: promoting aggressive therapy against tumours while carefully mapping patient-specific prognostic landscapes to increase both treatment precision and safety. Owing to the evolving background of medical treatment protocols, the exploration of valuable biomarkers has become increasingly pertinent.

On the basis of the aforementioned predictions, we conclude that the risk scoring model, which was constructed on the basis of DRLRs, provides valuable insights for R0 HCC patients. We developed a risk model composed of KDM4A-AS1, MKLN1-AS, and TMCC1-AS1, all of which serve as prognostic risk factors for R0 HCC patients. In future research, it is imperative to delve deeper into the molecular mechanisms underlying the role of DRLRs in HCC pathogenesis and progression. Given the identification of hub DRLRs with substantial implications for the prognostic landscape of R0 HCC, subsequent studies should focus on exploring the therapeutic potential of targeting these molecules. Specifically, the interaction of DRLRs with oncogenic pathways

and their impact on the tumour microenvironment warrants thorough investigation. Additionally, incorporating advanced omics techniques to explore the epigenetic regulation and posttranscriptional modifications of these DRLRs could provide valuable insights into their role in tumour dynamics. Expanding on the preliminary findings of drug sensitivity, further research should assess the efficacy of these drugs in clinical trials, explicitly examining the differential responses on the basis of DRLR expression levels. Ultimately, this could facilitate the development of precision medicine strategies, tailoring treatments on the basis of the DRLR-associated risk profiles in R0 HCC patients.

Limitations

Although our study innovatively developed a novel prognostic prediction model highlighting the applicability of three DRLRs in predicting the OS of patients with R0 resection status in HCC, it has several limitations that warrant cautious interpretation of the findings.

First, the retrospective nature of the study, which is largely based on archived data from existing databases, restricts our ability to control for potential bias introduced during data collection. Prospective validation using a multicentric, diverse patient cohort would be beneficial to confirm our results across different demographic and genetic backgrounds, further bolstering the external validity of our findings. Second, although our model demonstrates sound predictive capabilities within the specific subset of R0 HCC patients, its applicability and reliability across other subtypes of liver cancer remain to be evaluated. This limitation underscores the necessity of broader testing and model adjustments to cater universally to various HCC stages and conditions. Finally, although our in vitro cellular functional experiments confirmed that KDM4A-AS1, MKLN1-AS, and TMCC1-AS1 promote HCC cell proliferation, migration, and invasion, further research is needed to elucidate the specific mechanisms underlying how these lncRNAs induce malignant biological behaviour in HCC cells. By addressing these limitations in future research, the utility and robustness of the prognostic model can be significantly enhanced, contributing to more precise and individualized therapeutic strategies for HCC management.

Conclusions

In this comprehensive study, we developed and validated an innovative prognostic model anchored by three DRLRs, namely, KDM4A-AS1, MKLN1-AS, and TMCC1-AS1. This model exhibits robust predictive validity for OS among patients with HCC following complete (R0) resection. Our study revealed that

the identified signature is pertinent for patients with R0 hepatocellular carcinoma (HCC) across various age groups, tumour stages, and pathological features, establishing it as an independent prognostic factor. This research delineates critical biological pathways associated with the signature and enhances our understanding of the complexity within the tumour microenvironment. An increased presence of M0 macrophages and activated CD4 memory T cells as well as elevated expression of major histocompatibility complex (MHC) class I were observed in patients categorized as high risk. Furthermore, these patients exhibit increased levels of tumour immune dysfunction and exclusion (TIDE), mutation frequency, and tumour mutational burden (TMB). These factors collectively impact the response to various therapeutic interventions, indicating increased responsiveness to medications, including GDC0810, MK-8776, osimertinib, paclitaxel, and YK-4–279, in high-risk groups, thus providing insights for potential treatment options. Bioinformatics analysis also suggested that three pivotal DRLRs have significant prognostic importance and diagnostic value for R0 HCC. This information can guide more tailored and effective therapeutic approaches for managing R0 hepatocellular carcinoma. Moreover, our findings demonstrate that these three hub lncRNAs not only are prognostic biomarkers but also actively contribute to the pathophysiology of HCC by modulating tumour cell proliferation, migration, and invasion. This insight paves the way for targeted therapies that could disrupt these molecular mechanisms, offering hope for more personalized and effective treatment strategies for HCC patients.

Abbreviations

AFP	Alpha-fetoprotein
AI	Artificial intelligence
AKT	Protein kinase B
ATP	Adenosine 5′-triphosphate
AUC	Area under curve
BP	Biological process
CC	Cellular component
CI	Confidence interval
DRLRs	Disulfidptosis-related long noncoding RNAs
ECOG	Eastern cooperative oncology group
EdU	5-Ethynyl-2′-deoxyuridine
EMT	Epithelial–mesenchymal transition
ETS	E-twenty-six
FBS	Foetal bovine serum
FDR	False discovery rate
GAPDH	Glyceraldehyde-3-phosphate dehydrogenase
GO	Gene Ontology
GSEA	Gene set enrichment analysis
HCC	Hepatocellular carcinoma
HDGF	Hepatoma-derived growth factor
IC_{50}	Half maximal inhibitory concentration
ICI	Immune checkpoint inhibitor
IFN	Interferon
KM	Kaplan–Meier
LASSO	Least absolute shrinkage and selection operator
lncRNAs	Long noncoding RNAs
MF	Molecular function
MHC	Major histocompatibility complex
ML	Machine learning
NADPH	Nicotinamide adenine dinucleotide phosphate
NK	Natural killer
OS	Overall survival
PBS	Phosphate buffer saline
PCA	Principal component analysis
pDCs	Plasmacytoid dendritic cells
PFS	Progression-free survival
PI3K	Phosphoinositide 3-kinase
qRT-PCR	Quantitative real time polymerase chain reaction
RMH	Royal Marsden Hospital
RNA-seq	RNA sequencing
ROC	Receiver operating characteristic curve
RS	Risk score
siRNA	Small interfering RNA
ssGSEA	Single-sample gene set enrichment analysis
TCGA	The Cancer Genome Atlas
TIDE	Tumour immune dysfunction and exclusion
timeROC	Time-dependent ROC
TILs	Tumour infiltrating lymphocytes
TMB	Tumour mutational burden
TNM	Tumour node metastasis

Supplementary Information

The online version contains supplementary material available at https://doi.org/10.1186/s12885-024-12816-3.

Supplementary material 1.

Supplementary material 2.

Supplementary material 3.

Supplementary material 4.

Supplementary material 5.

Supplementary material 6.

Supplementary material 7.

Supplementary material 8.

Supplementary material 9.

Supplementary material 10.

Supplementary material 11.

Supplementary material 12.

Data availability

The datasets used and analyzed during the current study are available from the corresponding author upon reasonable request.

Gu *et al. BMC Cancer*   (2024) 24:1068

Page 18 of 19

Availability of data and materials
Any data and R script used in this study can be obtained from the corresponding author upon reasonable request. The final manuscript was read and approved by all the authors. In this study, publicly available datasets were analysed. These data are available from The Cancer Genome Atlas (https://portal.gdc.cancer.gov/).

Declarations

Ethics approval and consent to participate
All investigations conformed to the principles outlined in the Declaration of Helsinki and were obtained from the ethics committee of Jurong Hospital affiliated to Jiangsu University (JRSRMYY-2023–042). Informed consent was obtained from all participants in this study.

Consent for publication
All the authors have agreed to the content of the manuscript and agree to this submission.

Competing interests
The authors declare no competing interests.

Author details
[1]Department of Infectious Diseases, Jurong Hospital Affiliated to Jiangsu University, Zhenjiang, Jiangsu, China. [2]Department of Infectious Diseases, the First Affiliated Hospital of Anhui Medical University, Hefei, Anhui, China. [3]Department of Gastroenterology, The Affiliated Changzhou No.2 People's Hospital of Nanjing Medical University, 188 Gehu Road, Wujin District, Changzhou, Jiangsu, China. [4]Department of Oncology, The Fourth Affiliated Hospital of Nanjing Medical University, 298 Nanpu Road, Jiangbei New District, Nanjing, China.

References
1. Sung H, Ferlay J, Siegel RL, Laversanne M, Soerjomataram I, Jemal A, et al. Global cancer statistics 2020: GLOBOCAN estimates of incidence and mortality worldwide for 36 cancers in 185 countries. CA Cancer J Clin. 2021;71:209–49.
2. Yang JD, Hainaut P, Gores GJ, Amadou A, Plymoth A, Roberts LR. A global view of hepatocellular carcinoma: trends, risk, prevention and management. Nat Rev Gastroenterol Hepatol. 2019;16:589–604.
3. Yang YQ, Wen ZY, Liu XY, Ma ZH, Liu YE, Cao XY, et al. Current status and prospect of treatments for recurrent hepatocellular carcinoma. World J Hepatol. 2023;15:129–50.
4. Llovet JM, Castet F, Heikenwalder M, Maini MK, Mazzaferro V, Pinato DJ, et al. Immunotherapies for hepatocellular carcinoma. Nat Rev Clin Oncol. 2022;19:151–72.
5. Kulik L, El-Serag HB. Epidemiology and management of hepatocellular carcinoma. Gastroenterology. 2019;156:477–91.e1.
6. Scherber PR, Gäbelein G, Eisele RM, Igna D, Glanemann M. Early stage liver cancer : hepatocellular carcinoma. Chirurg. 2018;89:281–8.
7. Zhao HT, Cai JQ. Chinese expert consensus on neoadjuvant and conversion therapies for hepatocellular carcinoma. World J Gastroenterol. 2021;27:8069–80.
8. Erstad DJ, Tanabe KK. Prognostic and therapeutic implications of microvascular invasion in hepatocellular carcinoma. Ann Surg Oncol. 2019;26:1474–93.
9. Liu X, Nie L, Zhang Y, Yan Y, Wang C, Colic M, et al. Actin cytoskeleton vulnerability to disulfide stress mediates disulfidptosis. Nat Cell Biol. 2023;25:404–14.
10. Zhao S, Wang L, Ding W, Ye B, Cheng C, Shao J, et al. Crosstalk of disulfidptosis-related subtypes, establishment of a prognostic signature and immune infiltration characteristics in bladder cancer based on a machine learning survival framework. Front Endocrinol (Lausanne). 2023;14:1180404.
11. Hogg PJ. Biological regulation through protein disulfide bond cleavage. Redox Rep. 2002;7:71–7.
12. Wang Y, Jiang Y, Wei D, Singh P, Yu Y, Lee T, et al. Nanoparticle-mediated convection-enhanced delivery of a DNA intercalator to gliomas circumvents temozolomide resistance. Nat Biomed Eng. 2021;5:1048–58.
13. Gu X, Li H, Sha L, Zhao W. A prognostic model composed of four long noncoding RNAs predicts the overall survival of Asian patients with hepatocellular carcinoma. Cancer Med. 2020;9:5719–30.
14. Yang Z, Cao S, Wang F, Du K, Hu F. Characterization and prognosis of biological microenvironment in lung adenocarcinoma through a disulfidptosis-related lncRNAs signature. Genet Res. 2023;2023:6670514.
15. Fasihfar Z, Rokhsati H, Sadeghsalehi H, Ghadezadeh M, Gheisari M. AI-driven malaria diagnosis: developing a robust model for accurate detection and classification of malaria parasites. Iranian J Blood Cancer. 2023;15:112–24.
16. Ghadezadeh M, Asadi F, Ghorbani N, Almasi S, Taami T. Toward artificial intelligence (AI) applications in the determination of COVID-19 infection severity: considering AI as a disease control strategy in future pandemics. Iranian J Blood Cancer. 2023;15:93–111.
17. Liu L, Liu J, Lyu Q, Huang J, Chen Y, Feng C, et al. Disulfidptosis-associated LncRNAs index predicts prognosis and chemotherapy drugs sensitivity in cervical cancer. Sci Rep. 2023;13:12470.
18. Blackstone EH. Breaking down barriers: helpful breakthrough statistical methods you need to understand better. J Thorac Cardiovasc Surg. 2001;122:430–9.
19. Gu X, Sha L, Zhang S, Shen D, Zhao W, Yi Y. Neutrophils and lymphocytes can help distinguish asymptomatic COVID-19 from moderate COVID-19. Front Cell Infect Microbiol. 2021;11.
20. Maeser D, Gruener RF, Huang RS. oncoPredict: an R package for predicting in vivo or cancer patient drug response and biomarkers from cell line screening data. Brief Bioinform. 2021;22:bbab260.
21. Tsilimigras DI, Bagante F, Moris D, Hyer JM, Sahara K, Paredes AZ, et al. Recurrence patterns and outcomes after resection of hepatocellular carcinoma within and beyond the barcelona clinic liver cancer criteria. Ann Surg Oncol. 2020;27:2321–31.
22. Kim HI, An J, Kim JY, Shin HP, Park SY, Song GW, et al. Postresection period-specific hazard of recurrence as a framework for surveillance strategy in patients with hepatocellular carcinoma: a multicenter outcome study. Liver Cancer. 2022;11:141–51.
23. Pereira DJ, Schoolwerth AC, Pais VM. Cystinuria: current concepts and future directions. Clin Nephrol. 2015;83:138–46.
24. Elmonem MA, Veys KR, Soliman NA, van Dyck M, van den Heuvel LP, Levtchenko E. Cystinosis: a review. Orphanet J Rare Dis. 2016;11:47.
25. Min HY, Lee HY. Oncogene-driven metabolic alterations in cancer. Biomol Ther (Seoul). 2018;26:45–56.
26. Zheng P, Zhou C, Ding Y, Duan S. Disulfidptosis: a new target for metabolic cancer therapy. J Exp Clin Cancer Res. 2023;42:103.
27. Hadian K, Stockwell BR. The therapeutic potential of targeting regulated non-apoptotic cell death. Nat Rev Drug Discov. 2023;22:723–42.
28. Liu X, Zhuang L, Gan B. Disulfidptosis: disulfide stress-induced cell death. Trends Cell Biol. 2024;34:327–7.
29. Chen T, Liu R, Niu Y, Mo H, Wang H, Lu Y, et al. HIF-1α-activated long noncoding RNA KDM4A-AS1 promotes hepatocellular carcinoma progression via the miR-411-5p/KPNA2/AKT pathway. Cell Death Dis. 2021;12:1152.
30. Shen HM, Zhang D, Xiao P, Qu B, Sun YF. E2F1-mediated KDM4A-AS1 up-regulation promotes EMT of hepatocellular carcinoma cells by recruiting ILF3 to stabilize AURKA mRNA. Cancer Gene Ther. 2023;30:1007–17.
31. Zhou B, Wu Y, Cheng P, Wu C. Long noncoding RNAs with peptide-encoding potential identified in esophageal squamous cell carcinoma: KDM4A-AS1-encoded peptide weakens cancer cell viability and migratory capacity. Mol Oncol. 2023;17:1419–36.
32. Guo C, Zhou S, Yi W, Yang P, Li O, Liu J, et al. SOX9/MKLN1-AS axis induces hepatocellular carcinoma proliferation and epithelial-mesenchymal transition. Biochem Genet. 2022;60:1914–33.
33. Chen X, Ye Q, Chen Z, Lin Q, Chen W, Xie C, et al. Long non-coding RNA muskelin 1 antisense RNA as a potential therapeutic target in hepatocellular carcinoma treatment. Bioengineered. 2022;13:12237–47.
34. Pan G, Zhang J, You F, Cui T, Luo P, Wang S, et al. ETS proto-oncogene 1-activated muskelin 1 antisense RNA drives the malignant progression of hepatocellular carcinoma by targeting miR-22-3p to upregulate ETS proto-oncogene 1. Bioengineered. 2022;13:1346–58.

Gu *et al. BMC Cancer*   (2024) 24:1068

Page 19 of 19

35. Gao W, Chen X, Chi W, Xue M. Long non-coding RNA MKLN1-AS aggravates hepatocellular carcinoma progression by functioning as a molecular sponge for miR-654-3p, thereby promoting hepatoma-derived growth factor expression. Int J Mol Med. 2020;46:1743–54.

36. Zhao QJ, Zhang J, Xu L, Liu FF. Identification of a five-long non-coding RNA signature to improve the prognosis prediction for patients with hepatocellular carcinoma. World J Gastroenterol. 2018;24:3426–39.

37. Deng B, Yang M, Wang M, Liu Z. Development and validation of 9-long non-coding RNA signature to predicting survival in hepatocellular carcinoma. Medicine (Baltimore). 2020;99: e20422.

38. Cui H, Zhang Y, Zhang Q, Chen W, Zhao H, Liang J. A comprehensive genome-wide analysis of long noncoding RNA expression profile in hepatocellular carcinoma. Cancer Med. 2017;6:2932–41.

39. Fu Y, Si A, Wei X, Lin X, Ma Y, Qiu H, et al. Combining a machine-learning derived 4-lncRNA signature with AFP and TNM stages in predicting early recurrence of hepatocellular carcinoma. BMC Genom. 2023;24:89.

40. Chen C, Su N, Li G, Shen Y, Duan X. Long non-coding RNA TMCC1-AS1 predicts poor prognosis and accelerates epithelial-mesenchymal transition in liver cancer. Oncol Lett. 2021;22:773.

41. Belk JA, Daniel B, Satpathy AT. Epigenetic regulation of T cell exhaustion. Nat Immunol. 2022;23:848–60.

42. Wang L, Yan K, He X, Zhu H, Song J, Chen S, et al. LRP1B or TP53 mutations are associated with higher tumor mutational burden and worse survival in hepatocellular carcinoma. J Cancer. 2021;12:217–23.

43. Rizzo A, Ricci AD, Brandi G. Trans-Arterial Chemoembolization Plus Systemic Treatments for Hepatocellular Carcinoma: An Update. J Pers Med. 2022;12:1788.

44. Guven DC, Sahin TK, Erul E, Rizzo A, Ricci AD, et al. The association between albumin levels and survival in patients treated with immune checkpoint inhibitors: A systematic review and meta-analysis. Front Mol Biosci. 2022;9:1039121.

45. Sahin TK, Rizzo A, Aksoy S, Guven DC. Prognostic Significance of the Royal Marsden Hospital (RMH) Score in Patients with Cancer: A Systematic Review and Meta-Analysis. Cancers (Basel). 2024;16:1835.

46. Rizzo A, Mollica V, Tateo V, Tassinari E, Marchetti A, Rosellini M, et al. Hypertransaminasemia in cancer patients receiving immunotherapy and immune-based combinations: the MOUSEION-05 study. Cancer Immunol Immunother. 2023;72:1381–94.

47. Rizzo A, Santoni M, Mollica V, Logullo F, Rosellini M, Marchetti A, et al. Peripheral neuropathy and headache in cancer patients treated with immunotherapy and immuno-oncology combinations: the MOUSEION-02 study. Expert Opin Drug Metab Toxicol. 2021;17:1455–66.

Publisher's Note